




## Article

# Effect of Tropical Marine Atmospheric Environment on Corrosion Behaviour of the 7B04-T74 Aluminium Alloy

Ning Li <sup>1</sup>, Weifang Zhang <sup>2</sup>, Xiaojun Yan <sup>1</sup>, Meng Zhang <sup>3</sup>, Lu Han <sup>2</sup> and Yikun Cai <sup>4,\*</sup>

<sup>1</sup> School of Energy and Power Engineering, Beihang University, Beijing 100191, China; guess\_lining@buaa.edu.cn (N.L.); yanxiaojun@buaa.edu.cn (X.Y.)

<sup>2</sup> School of Reliability and Systems Engineering, Beihang University, Beijing 100191, China; 08590@buaa.edu.cn (W.Z.); hanlu13051827622@buaa.edu.cn (L.H.)

<sup>3</sup> Space Environment and Reliability Division, Beijing Institute of Spacecraft System Engineering, Beijing 100094, China; zhangmeng123@buaa.edu.cn

<sup>4</sup> School of Aeronautics and Astronautics, Sichuan University, Chengdu 610065, China

\* Correspondence: caiyikun@scu.edu.cn

**Abstract:** In this work, the effects of the tropical marine atmospheric environment on the corrosion behaviour of the 7B04-T74 aluminium alloy were systematically investigated by using accelerated testing, together with corrosion kinetic analysis, microstructure observation, product composition analysis, and potentiodynamic polarization curve tests. The weight loss method was used for the corrosion kinetics analysis. The surface morphology and corrosion products transformation law were investigated by OM, SEM, EDS, and XPS. The electrochemical characteristics were studied using potentiodynamic polarization curves. The research indicated that the 7B04-T74 aluminium alloy has eminent corrosion resistance in the tropical marine atmospheric environment. Localized pitting corrosion occurred rapidly in the tropical marine atmosphere. In the later stage of corrosion, the corrosion of aluminium alloy did not become serious. Specifically, no obvious intergranular corrosion was found, which is related to the thermal treatment method. Corrosion products included  $\text{Al}(\text{OH})_3$ ,  $\text{Al}_2\text{O}_3$ , and  $\text{AlCl}_3$ , of which  $\text{Al}(\text{OH})_3$  is the most notable.

**Keywords:** aluminium alloy; tropical marine atmosphere; corrosion behavior



**Citation:** Li, N.; Zhang, W.; Yan, X.; Zhang, M.; Han, L.; Cai, Y. Effect of Tropical Marine Atmospheric Environment on Corrosion Behaviour of the 7B04-T74 Aluminium Alloy. *Metals* **2023**, *13*, 995. <https://doi.org/10.3390/met13050995>

Academic Editor: Branimir N. Grgur

Received: 8 April 2023

Revised: 10 May 2023

Accepted: 11 May 2023

Published: 21 May 2023



**Copyright:** © 2023 by the authors. Licensee MDPI, Basel, Switzerland. This article is an open access article distributed under the terms and conditions of the Creative Commons Attribution (CC BY) license (<https://creativecommons.org/licenses/by/4.0/>).

## 1. Introduction

Over 70% of the Earth's surface is covered by oceans, and abundant marine resources provide a large number of valuable and vital ecosystem services for human well-being, such as climate regulation, food, energy, minerals, genetic resources, and even cultural and recreational services [1]. From the perspectives of politics, economics, and safety, the construction of marine engineering and equipment has become essential to promote the development and utilization of the ocean. As a result, it also imposes higher developmental requirements on the environmental adaptability and durability of materials.

Aluminium alloys are used extensively in the marine equipment and aircraft industries due to their excellent properties, such as high strength and remarkable corrosion resistance [2,3]. Among them, 7-series aluminium alloy, as a kind of ultra-high strength aluminium alloy series, is widely used in the manufacturing of aircraft load-bearing parts, such as the frame, beam, and girder, and is one of the most prominent structural materials in the field of aircraft structure [4,5]. The composition and thermal treatment process of aluminium alloys can affect their corrosion resistance [6]. Compared with 7075 aluminium alloy, the 7B04 aluminium alloy contains Cr, which can improve its toughness and corrosion resistance [7].

Currently, the main way to study the corrosion mechanisms of materials is to carry out exposure tests in the actual service environments. Zhao et al. investigated the 7A85 aluminium alloy in industrial-marine atmospheric environments for 5 years [8]. The

pitting corrosion of the 7A85 aluminium alloy gradually shifted to intergranular corrosion, severely reducing its mechanical properties. Sun et al. studied the long-term atmospheric corrosion behavior of the 2024 and 7075 aluminium alloys in urban, coastal, and industrial environments [9]. The results showed that exfoliation corrosion occurred in coastal and industrial atmospheres, and the extruded 2024 aluminium alloy suffered severe exfoliation and rapid deterioration of mechanical properties in a coastal atmosphere. Zhang et al. investigated the surface and sectional corrosion behavior of anodized 2024-T4 exposed to a coastal environment for 7 years and 20 years [10]. After conducting extensive field exposure tests, this test method suffers from obvious shortcomings such as prolonged cycles, excessive cost, and, most importantly, the inability to accurately assess the impact of individual environmental factors on the corrosion mechanism [11,12].

Therefore, a large number of accelerated tests have been proposed to study the atmospheric corrosion of aluminium alloys. Due to the controllable conditions of accelerated tests, it is highly efficient in studying the corrosion behavior and mechanisms of materials under independent environmental factors, specific pollutants, or special environments [13,14]. Dan et al. used the results of the 7-day dew point corrosion test to demonstrate that the results were similar to the results of the 3-month coastal exposed test, proving that the dew point corrosion test can effectively reproduce and accelerate the marine atmospheric corrosion of aluminium alloys [15]. Vera et al. studied the effects of individual environment factors, such as relative humidity, temperature, atmospheric pollutants, and Cl<sup>-</sup> concentrations on the corrosion behaviours of the 2A12 and AA6201 aluminium alloys [16]. Cao et al. investigated the corrosion behavior of the 2A02 Al alloy in a simulated marine atmosphere, and the results showed that the mass-gain increases gradually during the corrosion time, while the corrosion rate decreases [17]. Peng et al. found extruded 6061 aluminium alloy incurred severe intergranular and intragranular corrosion in a simulated Nansha marine atmosphere using wet-dry cyclic accelerated tests [18]. However, the corrosion mechanism and behavior of the 7-series aluminium alloy in the tropical marine atmosphere is still under investigation.

Hence, the effects of the tropical marine atmospheric environment on the corrosion behavior of the 7B04-T74 aluminium alloy were systematically investigated by using accelerated tests, together with corrosion kinetic analysis, microstructure observation, product composition analysis, and potentiodynamic polarization curve tests. The weight loss method was used for the corrosion kinetics analysis. The surface morphology and corrosion products transformation law were investigated by OM, SEM, EDS, and XPS. The electrochemical characteristics were studied using potentiodynamic polarization curves.

## 2. Experimental Methods and Procedures

### 2.1. Experimental Material

The chemical composition of the 7B04-T74 aluminium alloy supplied by Northeast Light Alloy Co., Ltd. (Shenyang, China) is shown in Table 1. Table 2 shows the thermal treatment process parameters of T74.

**Table 1.** Chemical compositions of the 7B04-T74 aluminium alloy.

Element	Zn	Mg	Cu	Ni	Ti	Cr	Mn	Fe	Si	Al
Composition (wt%)	6.09	2.54	1.65	<0.05	0.017	0.13	0.26	0.14	0.049	Bal.

**Table 2.** The thermal treatment process parameters of T74.

Thermal Treatment Procedure	Temperature (°C)	Time
Solution Treatment Process	470	35 min
Primary Aging Treatment Process	115	7 h
Secondary Aging Treatment Process	165	16 h

The specimen size is 50 mm × 50 mm × 3 mm, with a surface roughness of 1.6. The number of specimens retrieved at each sampling time is 3. The specimens were rinsed with acetone and deionized water, then dried in a drying oven at 80 °C and intended for the alternate immersion test, corrosion kinetic analysis, surface morphology observation, and corrosion product composition identification.

The specimens for potentiodynamic polarization curves analysis are packaged in epoxy resin. The exposed working face size is 10 mm × 10 mm, with a surface roughness of 1.6. These specimens were tested with potentiodynamic polarization curves directly after the alternate immersion test without drying. The number of parallel specimens is 3.

## 2.2. Alternate Immersion Test

In the case of drawing on ISO 11130:2017, the alternate immersion test for the 7B04-T74 aluminium alloy was carried out for 576 h in a simulated tropical marine atmospheric environment. The dry-wet cycle ratio for the test was 3:1, which means that the immersion and drying time were 15 min and 45 min, respectively. The drying temperature and humidity are 40 ± 1 °C and 85% ± 1%, respectively. The corrosive solution maintained 4 wt% of Cl<sup>-</sup> to simulate the tropical marine atmospheric environment, and the chemical compositions of reagents are listed in Table 3. The pH value was 8.2 revised by 0.1 mol/L NaOH solution. Sampling time was 48 h, 96 h, 144 h, 288 h, 432 h, and 576 h. The specimens were dehydrated in a drying oven at 85 °C for 2 h for the subsequent tests.

**Table 3.** Chemical compositions of the corrosive solution, g/L.

NaCl	MgCl <sub>2</sub> ·6H <sub>2</sub> O	Na <sub>2</sub> SO <sub>4</sub>	CaCl <sub>2</sub>	KCl
37.2	16.67	6.14	1.74	1.04

## 2.3. Corrosion Kinetic Analysis

The corrosion kinetic analysis was characterized by weight loss method. Before the alternate immersion test, the weight ( $m_j$ ) of the specimens were measured by digital balance. After the alternate immersion test, the specimens were cleaned in nitric acid to remove the corrosion products, referring to the GB/T 16545-2015 standard. After that, the specimens were cleaned with acetone and subsequently dehydrated in a drying oven, after which the weight ( $m_i$ ) of the corroded specimens was measured. For precision, all measurements were repeated three times. The weight change was amended by the weight loss from a blank specimen that had undergone the pickling process only. The corrosion depth ( $D$ ) and corrosion rate ( $v_{\text{corr}}$ ) were used to analyse the corrosion kinetic. The equation below was used to calculate the corrosion depth ( $D$ ):

$$D = \frac{m_j - m_i - m_b}{\rho S} \quad (1)$$

where  $m_j$  and  $m_i$  are the weight (g) before the alternate immersion test and after the acid washing process, respectively.  $m_b$  is the mass loss during the acid washing process which is tested by blank specimens.  $\rho$  is the density of aluminium alloy (2.79 g/cm<sup>3</sup>), and  $S$  is the surface area (cm<sup>2</sup>) of the specimens.

The equation below was used to calculate the corrosion rate ( $v_{\text{corr}}$ ):

$$v_{\text{corr}} = \frac{D}{t} \quad (2)$$

where  $D$  is the corrosion depth (µm) and  $t$  is the corrosion time (h).

## 2.4. Surface Morphology Observation

The digital camera (Nikon D50) (Nikon Corporation, Tokyo, Japan) was used to record the macroscopic morphology and the colour, state, and adhesion of the corrosion product. The microscopic morphology and element distribution were studied and detected

by SEM (Zeiss Supra55) (Carl Zeiss Meditec AG, Jena, Germany) and EDS (Oxford X-ray Spectrometer) (Oxford Instruments plc, Abingdon, UK).

### 2.5. Corrosion Product Composition Identification

The identification of the corrosion products was analysed using XPS (Thermo EscaLab 250XI) (Thermo Fisher Scientific, Waltham, MA, USA). Under the voltage and current conditions of 14.8 kV and 1.6 A, the corrosion products were scanned by X-ray with power of 150 W and a beam spot of 650  $\mu\text{m}$  (Al Ka = 1486.6 eV). The wide sweep range was 100 eV, the narrow sweep range was 20 eV, and the narrow sweep elements were Al, Cl, and O. Polluted carbon C1s (284.8 eV) was used for charge correction of the data. The software used for processing the XPS data was XPS Peak 1.

### 2.6. Potentiodynamic Polarization Curves Analysis

The potentiodynamic polarization was tested by using a standard three-electrode system at room temperature on a workstation (DH7000) (Jiangsu Donghua Analytical Instruments Co., Ltd., Jingjiang, China), as shown in Figure 1. The working electrode was the 7B04-T74 aluminium alloy, and Ag/AgCl/KCl (Sat'd) reference electrodes were used while a platinum sheet was used as the auxiliary electrode. The test solution is a 3.5 wt% NaCl solution, and the specimens were immersed in the solution for 3 min to maintain a stationary open-circuit voltage. The applied potential ranges from plus to minus 0.5 volts, with respect to the open-circuit potential, and has a sweep rate of 1 mV/s.

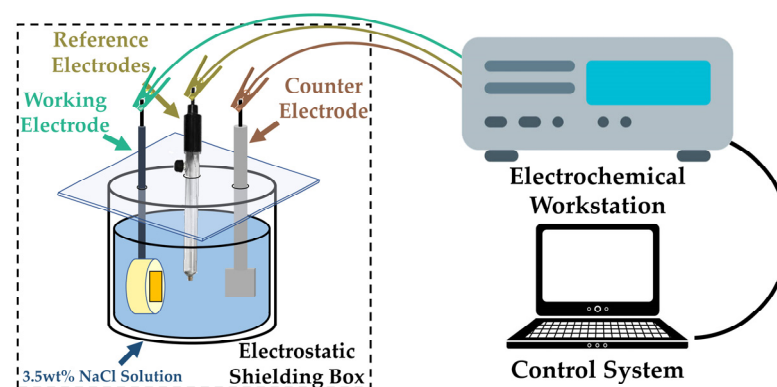


**Figure 1.** Schematic diagram of potentiodynamic polarization curve test.

## 3. Results and Discussion

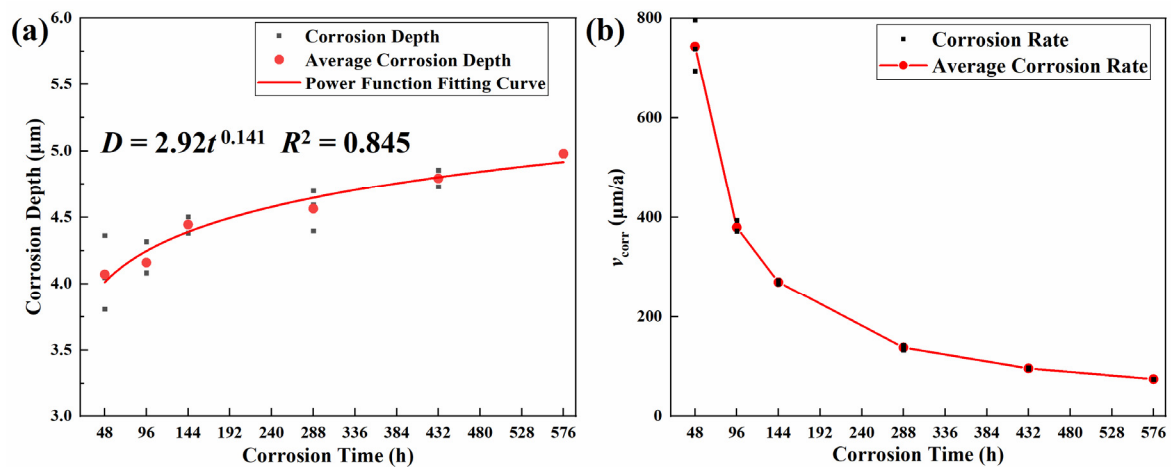
### 3.1. Corrosion Kinetic Analysis

Figure 2 shows the results of the corrosion kinetics analysis of the 7B04-T74 aluminium alloy after 576 h corrosion. The general power function equation  $D = At^n$  is widely utilized to fit the atmospheric corrosion weight loss data of metallic materials, as demonstrated by several studies [19], where  $D$  is the corrosion depth ( $\mu\text{m}$ ),  $t$  is the corrosion time (h), and  $A$  and  $n$  are the fitting constants. As shown in Figure 2a, the corrosion depth data obtained from the alternating immersion test can be well fitted by the power function model. The weight loss was increased by the extended corrosion time; nevertheless, its rising tendency was slowing. The regression model for the corrosion depth data is as follows:

$$D = At^n = 2.92t^{0.141} \quad (3)$$

The constant  $n$  can reflect the corrosion tendency of metal materials, and its value is normally inversely proportional to the corrosion resistance [20,21]. The constant  $n$  fitted to the corrosion weight loss data for the 7B04-T74 aluminium alloy is 0.141, which indicates that the corrosion of this grade of aluminium alloy presents a decelerating process under the simulated marine atmospheric environment, and also represents its excellent corrosion resistance. The constant  $A$  is frequently used to indicate the corrosion tendency of a

metal material. The fitting constant  $A$  of the corrosion weight loss data for the 7B04-T74 aluminium alloy is 2.92, indicating that the aluminium alloy is not susceptible to corrosion in the tropical marine atmospheric environment.



**Figure 2.** Calculated corrosion depth (a) and corrosion rate (b) of the 7B04-T74 aluminium alloy.

### 3.2. Surface Morphology Analysis

#### 3.2.1. Macroscopic Morphology Analysis

Figure 3 shows the surface morphology of the 7B04-T74 aluminium alloy without corrosion, after 48 h and 576 h. From Figure 3a, the uncorroded sample has a smooth surface and metallic lustre due to its surface roughness of 1.6. Then, local pitting corrosion appeared on the surface after 48 h in Figure 3b. Visually, white corrosion products are deposited around the pit area. The typical form of local corrosion of aluminium alloy is pitting corrosion. When  $\text{Cl}^-$  contacts the aluminium alloy surface, the cause of pitting corrosion is mainly due to passivation breakdown, and the possible corrosion mechanisms include penetration, adsorption, and film breaking [22]. The second phase contained in aluminium alloys is a priority region of pitting [23,24]. After 576 h, the corrosion products increased around the pitting in Figure 3c, and the aluminium alloy's metallic lustre was lost. Nonetheless, the corrosion is still dominated by localized pitting corrosion after 576 h, as evidenced by the residual intact surface.

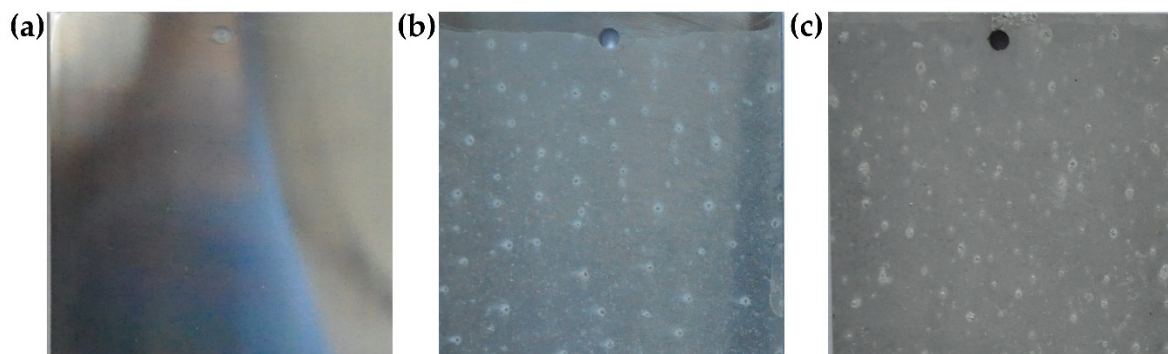


**Figure 3.** The surface morphology of uncorroded (a), after 48 h (b) and 576 h (c) of the 7B04-T74 aluminium alloy.

#### 3.2.2. Microscopic Morphology Analysis

Figure 4 shows the metallographic morphology of the uncorroded 7B04-T74 aluminium alloy. It can be seen that the surface contains a large number of second phase inclusions. Most intermetallic compound particles are not uniformly distributed within the grain, and a small number exist outside the grain boundaries. These inclusions mainly

contain elements such as Cu, Fe, and Mg. The addition of these elements improves the mechanical properties of the aluminium alloy while the corrosion resistance of the aluminium alloy is affected by the second phase induced by these elements due to the different potentials between the second phase and the matrix [25,26]. According to the study of He [27], the inclusions of—series aluminium alloy are microscale intermetallic particles mainly composed of  $Al_7Cu_2Fe$  phase, accompanied by a small amount of S-phase ( $Al_2CuMg$ ) and Fe-containing impurity phase ( $FeAl_3$ ).

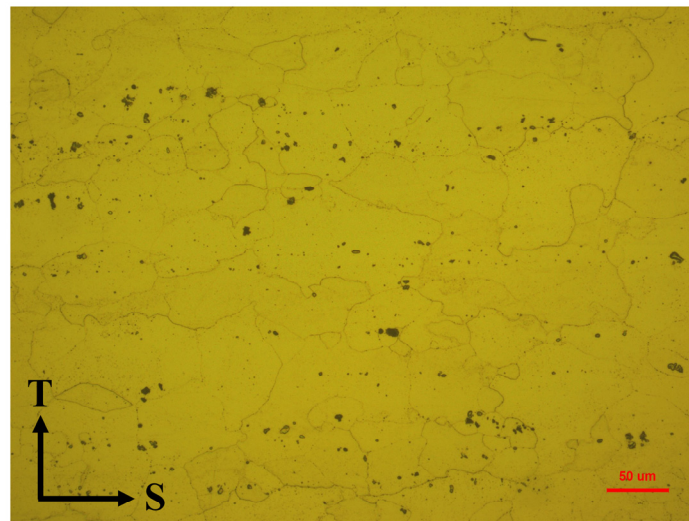


**Figure 4.** The metallographic morphology of the uncorroded 7B04-T74 aluminium alloy.

The microscopic surface morphology of the 7B04-T74 aluminium alloy after 48 h and 576 h of corrosion is shown in Figure 5. Localized pitting corrosion occurred on the surface after 48 h in Figure 5a. The integrity of the surface structure was maintained in all areas except those where pitting corrosion occurred. Corrosion products were deposited around the pitting with cracks caused by the water-loss effect. The oxide film of the aluminium alloy was attacked by halogen ions in the environment. The integrity of the surface was destroyed by the dissociation of the intermetallic particles. As shown in Figure 5b, the pitting was irregular and accompanied by longitudinal cracks. After 576 h, with the extension of corrosion time, corrosion gradually developed, corrosion products increased, and the size of the pitting increased in Figure 5c, which was consistent with the visual results. At the same time, the corrosion products gradually aggregated, forming a cluster of corrosion products. Inside the pitting, the accumulation of corrosion products could be observed with the cracks extending into the matrix in Figure 5d. It is worth noting that the aggregation of corrosion products is extremely inhomogeneous due to the fact that only localized corrosion occurred on the surface.

As shown in Figure 6, after 48 h of corrosion, EDS point scanning was performed on the corrosion products (No. 1) attached around the pitting pit and the uncorroded area (No. 2). The contents of O, Na, Cl, and other elements in the corrosion products were significantly increased compared with those in the uncorroded area, indicating that  $Cl^-$  directly participated in the corrosion reaction to form corrosion products containing  $Cl^-$ . In Figure 7, EDS surface scanning was performed on the corrosion products after 576 h of corrosion. O, Al, Na, Cl, and additional elements were enriched in the corrosion products, which also proved that  $Cl^-$  took part in the corrosion reaction and formed corrosion products containing  $Cl^-$ .

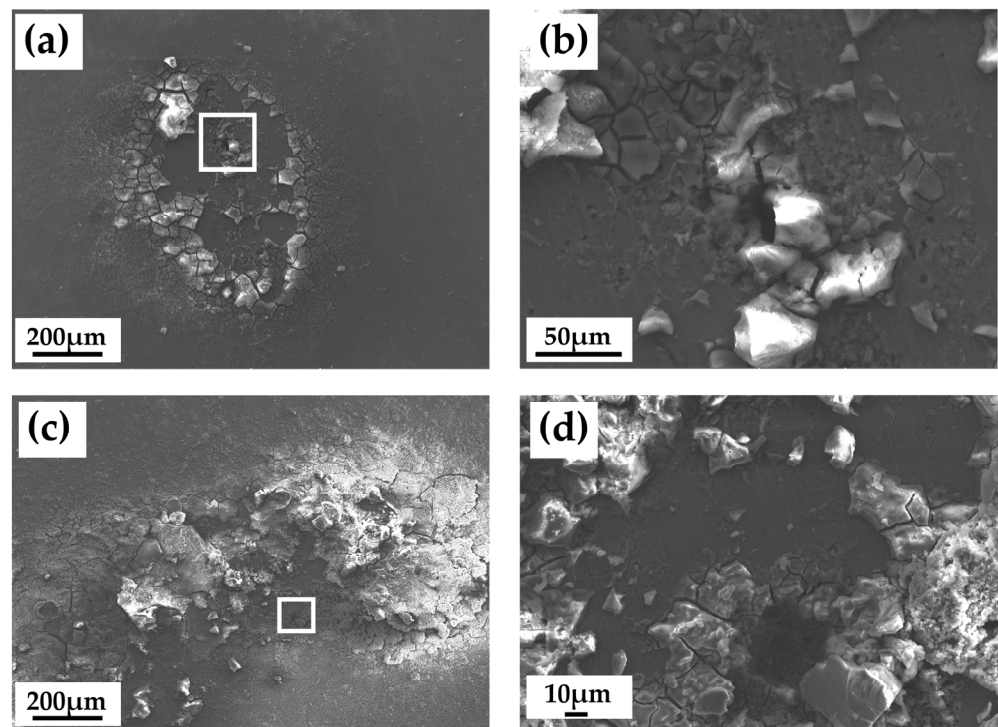


**Figure 5.** The surface morphology of the 7B04-T74 aluminium alloy corroded for 48 h (a) and 576 h (c), where (b) is the enlarged image of (a), (d) is the enlarged image of (c).

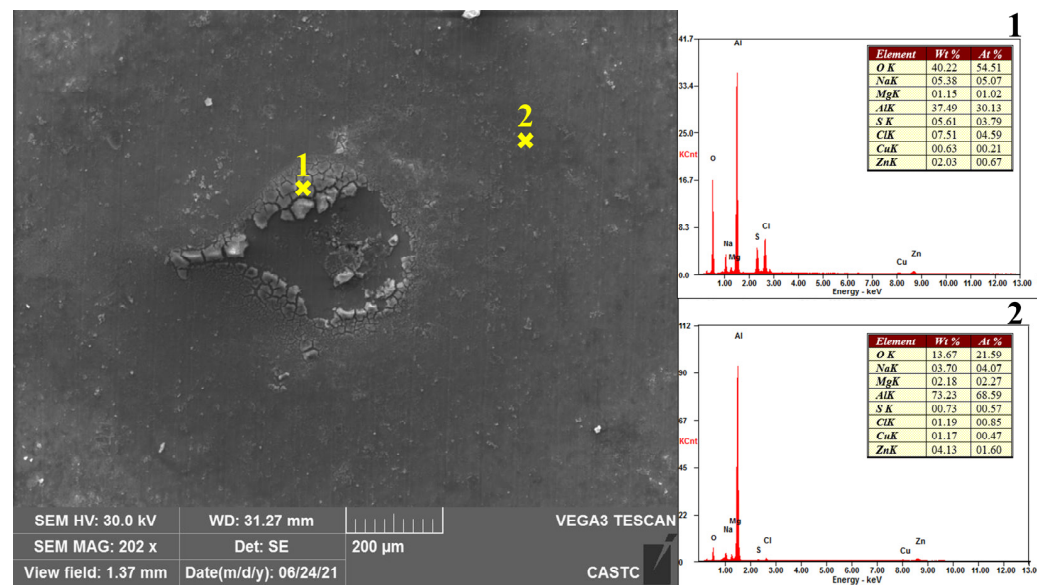


**Figure 6.** The EDS point scanning of the 7B04-T74 aluminium alloy corroded for 48 h.

As mentioned above, pitting corrosion is the main corrosion form in the aluminium alloys when used in tropical marine atmospheric environments. After the 576 h accelerated test, no obvious intergranular corrosion or exfoliation corrosion was observed. The oxide film is broken down by  $Cl^-$  in the marine atmosphere. Subsequently, the second phase particles undergo electrochemical reactions due to the potential differences with the matrix, which appear as pitting with short cracks in morphological surface observations.

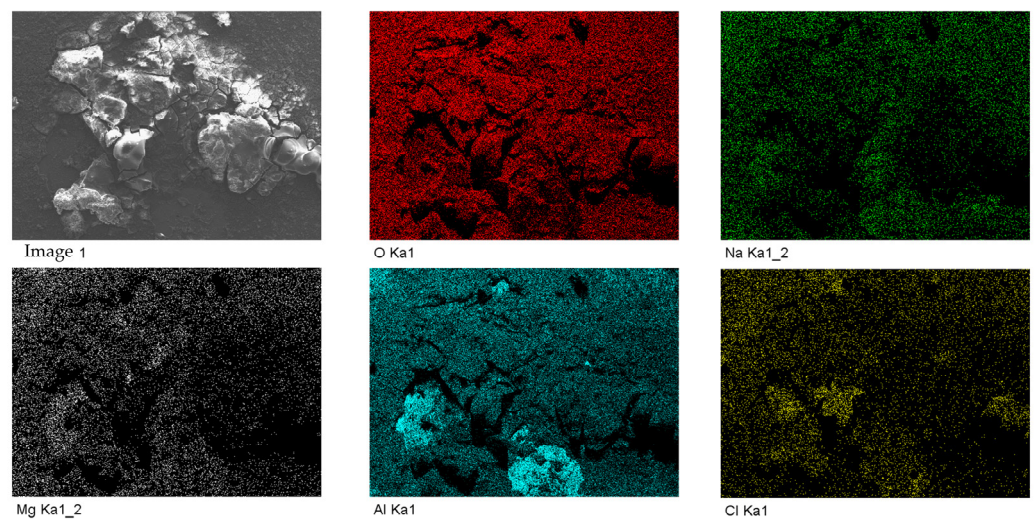


**Figure 7.** The EDS surface scanning results of the 7B04-T74 aluminium alloy after 576 h of corrosion.

### 3.3. Corrosion Product Composition Identification

XPS was used to identify the chemical composition of the corrosion products at different corrosion times. As an example, the XPS data of the corrosion products of the 7B04-T74 aluminium alloy corroded for 48 h are used to illustrate the composition and relative content of the corrosion product. The total XPS spectrogram of the corrosion products after 48 h is shown in Figure 8, where elements such as Al, C, O, and Cl can be detected.

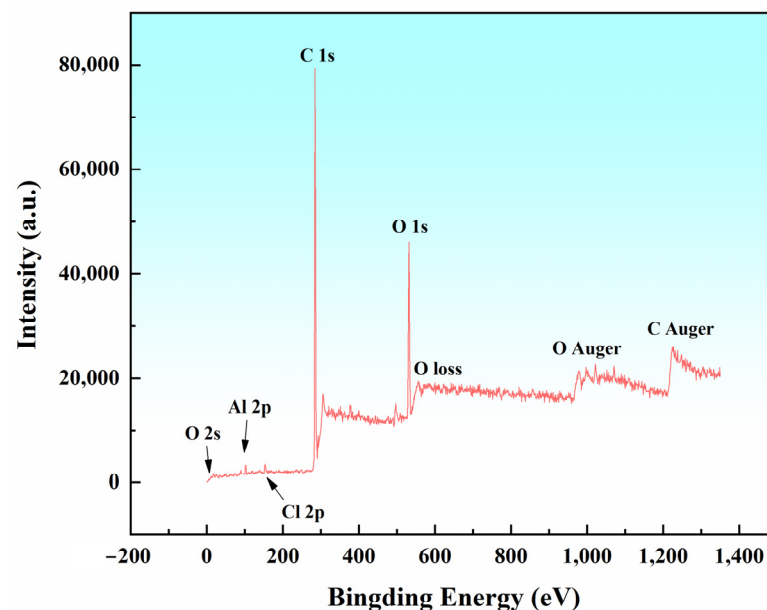


**Figure 8.** Total XPS spectrogram of the corrosion products of the 7B04-T74 aluminium alloy after 48 h of corrosion.

The XPS spectrograms of corrosion products of 7B04-T74 aluminium alloy corroded for 48 h are shown in Figure 9, and the high-resolution spectrograms of Al2p, O1s, and Cl2p orbitals are shown in Figure 9a–c, respectively. The spectrum of Al2p consists of three peaks, Al<sub>2</sub>O<sub>3</sub> (73.5 eV), Al(OH)<sub>3</sub> (74.3 eV), and AlCl<sub>3</sub> (75.3 eV). The O1s map also has three peaks at 530.5 eV, 531.7 eV, and 532.8 eV, which are used to estimate the oxygen content of aluminium oxide (O<sup>2-</sup>), hydroxide (OH<sup>-</sup>), and hydrate (H<sub>2</sub>O) in the corrosion products. Cl<sup>-</sup> is detected at 198.6 eV as metallic chlorine, AlCl<sub>3</sub>. Al(OH)<sub>3</sub> is the main component of the corrosion products.



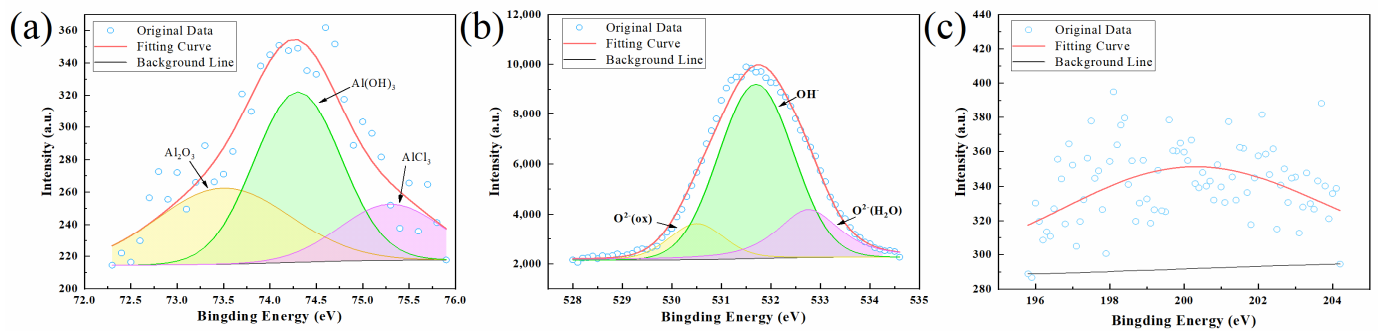


**Figure 9.** XPS spectrogram for (a) Al2p, (b) O1s, and (c) Cl2p of the corrosion products after 48 h.

In Figure 10, the relative content of corrosion products of the 7B04-T74 aluminium alloy under different corrosion times is given. It can be seen that Al(OH)<sub>3</sub> is the main product, and its content fluctuates around 50% with the increase in corrosion time. For AlCl<sub>3</sub>, there is a slow rising trend with increasing corrosion, which corresponds to a decreasing trend for Al<sub>2</sub>O<sub>3</sub>.

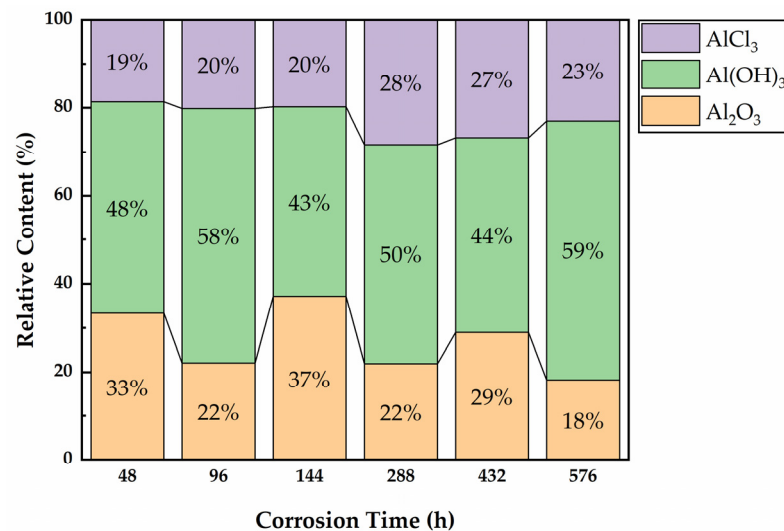


**Figure 10.** Relative content of the corrosion products of the 7B04-T74 aluminium alloy under different corrosion times.

### 3.4. Potentiodynamic Polarization Curves Analysis

Potentiodynamic polarization curves under different corrosion times are shown in Figure 11, and the parameters deduced are listed in Table 4.

**Table 4.** Electrochemical parameters of the potentiodynamic polarization curves.

Corrosion Time (h)	0	48	96	144	288	432	576
$i_{\text{corr}}$ ( $\mu\text{A}/\text{cm}^2$ )	42.0146	10.5536	0.4782	4.0365	16.2705	3.3814	2.7887
$E_{\text{corr}}$ (V)	−1.1720	−1.1543	−0.9403	−1.1196	−1.1396	−0.6643	−0.9882
$\beta_a$ (mV/decade)	237	250	130	127	274	26	114
$\beta_c$ (mV/decade)	−98	−81	−72	−71	−93	−320	−77
$R_p$ ( $\Omega\cdot\text{cm}^2$ )	717.47	2520.40	42,130.5	4905.34	1855.41	3091.86	7165.3

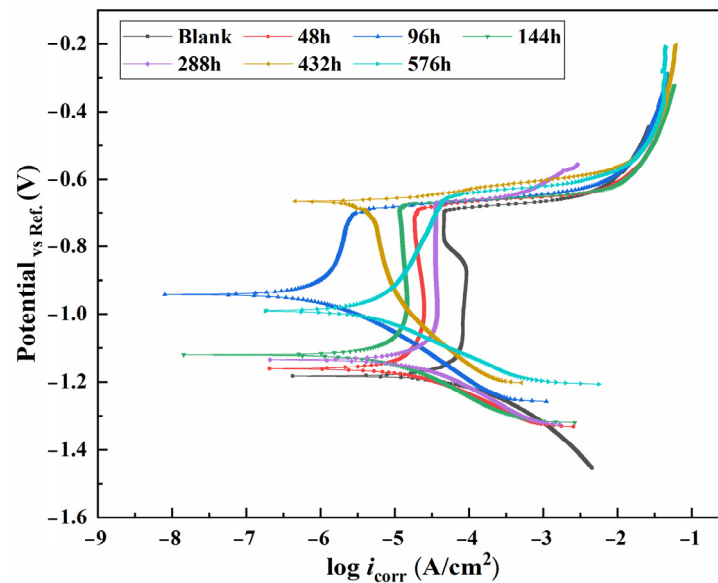


Figure 11. Potentiodynamic polarization curves after different corrosion times.

The anode regions of the polarization curves have distinct passivation zones and pitting potentials, with essentially the same value of the pitting potential. The similar shapes of the polarization curves demonstrate that the corrosion mechanism of the 7B04-T74 aluminium alloy does not change. The passivation zone disappears in the electrochemical sample curve after 432 h of corrosion, and the corrosion potential is the same as that of the pitting potential, indicating that the specimen's surface oxide film is in the state of breakdown when the potentiodynamic polarization curve is tested, and the corrosive medium can directly attack the aluminium alloy matrix through the oxide film. The anodic Tafel slope is lower after 432 h than other corrosion times. The lower the slope, the lower the reaction resistance, the higher the corrosion rate, and the easier it is to corrode.

As the corrosion time increases, the corrosion potential moves forward and gradually increases from  $-1.17$  V to  $-0.94$  V, but the overall fluctuation range is not large. This means that the corrosion of the sample gradually produces a suppression effect. Combined with the relevant conclusions of surface morphology observation, it can be shown that in the tropical marine atmospheric environment, the 7B04-T74 aluminium alloy is always dominated by pitting corrosion, and that the second phase particles contained on the surface gradually dissolve in the corrosive medium as the corrosion time increases. The corrosion rate is steadily decreasing. The corrosive medium did not penetrate to the interior of the aluminium alloy, so no obvious intergranular or exfoliation corrosion was found. The corrosion current of the uncorroded electrochemical specimen is  $42.0146 \mu\text{A}/\text{cm}^2$ , while that of the corroded 7B04-T74 aluminium alloy invariably fluctuates around  $10 \mu\text{A}/\text{cm}^2$ . The  $R_p$  value of the 7B04-T74 aluminium alloy also increased from 717.47 to several thousand, increasing by at least one order of magnitude. These two points can also prove that the pitting corrosion which occurs on the 7B04-T74 aluminium alloy is difficult to develop further in the marine atmosphere.

### 3.5. Corrosion Behavior Analysis

The corrosion mechanism and behavior of the 7B04-T74 aluminium alloy in tropical marine atmospheres were obtained by a combination of corrosion kinetics analysis, surface morphology observation, corrosion product composition analysis, and electrochemical analysis. The 7B04-T74 aluminium alloy contains many second phase or eutectic Si phase, which is cathode or anode relative to the matrix. Under extreme relative humidity, the surface absorbs a large amount of water vapor and forms a thin liquid film. When the thickness of the liquid film reaches a certain stage, the 7B04-T74 aluminium alloy begins to react with the ions in the film due to the potential difference between the second phase

particles and the substrate. For particles with higher Mg content, the potential is more negative than the matrix, so that the particles themselves dissolve, while for particles with higher Fe and Cu content, the potential is more positive, so that the matrix around the particles undergoes anodic dissolution. In the marine atmosphere, these electrochemical reactions are more easily induced due to the presence of  $\text{Cl}^-$ .

The corrosion mechanism of the 7B04-T74 aluminium alloy in the tropical marine atmosphere is shown in Figure 12. When the corrosion starts to occur, the  $\alpha$ -Al matrix will undergo anodic dissolution due to the dissolution of the intermetallic particles or the REDOX reaction between the second phase particles and matrix. The reaction process is as follows: the anodic process;  $\text{Al} - 3\text{e} \rightarrow \text{Al}^{3+}$ , while the cathode process;  $\text{O}_2 + 4\text{e} + 2\text{H}_2\text{O} \rightarrow 4\text{OH}^-$  (oxygen absorption reaction) and  $2\text{H}_2\text{O} + 2\text{e} \rightarrow 2\text{OH}^-$  (hydrogen evolution reaction). Then,  $\text{Al}^{3+}$  and  $\text{OH}^-$  in the environment undergo a secondary reaction to form  $\text{Al}(\text{OH})_3$ . At the same time, part of the reaction leads to the formation of an inert alumina film  $\text{Al}_2\text{O}_3$ , which makes the aluminium alloy passivated. In the tropical marine atmospheric environment, the oxide film of the aluminium alloy is susceptible to penetration in incomplete or defective regions due to the rich  $\text{Cl}^-$  which is easy to adsorb. The  $\text{Cl}^-$  in the corrosive medium will also participate in the electrochemical reaction; the reaction process includes  $\text{Al}(\text{OH})_3 + \text{Cl}^- \rightarrow \text{Al}(\text{OH})_2\text{Cl} + \text{OH}^-$ ,  $\text{Al}(\text{OH})_2\text{Cl} + \text{Cl}^- \rightarrow \text{Al}(\text{OH})\text{Cl}_2 + \text{OH}^-$ , and  $\text{Al}(\text{OH})\text{Cl}_2 + \text{Cl}^- \rightarrow \text{AlCl}_3 + \text{OH}^-$ . However, in the T74 thermal treatment,  $\eta'$  and  $\eta$  phase particles at the grain boundary aggregate and spheroidise, resulting in a larger size of these intergranular precipitates [6,28,29]. In contrast to the fine intergranular precipitate of T6 thermal treatment, it effectively blocks the anode corrosion channel at the grain boundaries, preventing the corrosive medium from attacking the aluminium alloy matrix along the grain boundaries and significantly improving the intergranular corrosion resistance of 7B04 aluminium alloy.

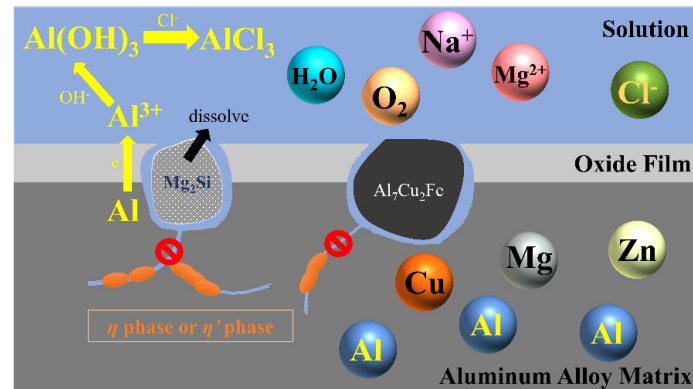


**Figure 12.** The corrosion mechanism of the 7B04-T74 aluminium alloy in the tropical marine atmosphere.

#### 4. Conclusions

The corrosion behavior and mechanism of the 7B04-T74 aluminium alloy in tropical marine atmospheric environments were studied using the 576 h alternate immersion test. A detailed study revealed the following:

1. The corrosion kinetics of the 7B04-T74 aluminium alloy followed the power functions  $D = At^n = 2.92t^{0.141}$ , which attests that this aluminium alloy has high corrosion resistance in the tropical marine atmospheric environment;
2. Due to the abundance of  $\text{Cl}^-$  in the marine atmospheric environment, the surface of the 7B04-T74 aluminium alloy undergoes rapid pitting corrosion. However, no significant intergranular or exfoliation corrosion was found while the corrosion time increased, which proves that the T74 thermal treatment process could be a successful means of improving the intergranular corrosion resistance of the 7B04-T74 aluminium alloy;
3. The corrosion products of the 7B04-T74 aluminium alloy gradually accumulate around the pitting, forming a cluster. The corrosion products were  $\text{Al}_2\text{O}_3$ ,  $\text{Al}(\text{OH})_3$ , and  $\text{AlCl}_3$ .

- The detection of  $\text{Cl}^-$  in the form of metallic chlorine,  $\text{AlCl}_3$ , proves that chlorine ions in the marine atmosphere are involved in the corrosion reaction of the 7B04-T74 aluminium alloy.  $\text{Al}(\text{OH})_3$  is the main component of surface corrosion products;
4. The similar shape of the potentiodynamic polarization curves at different corrosion times proves that the corrosion mechanism of the 7B04-T74 aluminium alloy does not change. The pitting potential is clearly observed in the curves, which proves that the oceanic atmospheric corrosion of the 7B04-T74 aluminium alloy remains in the pitting stage. The forward motion of the corrosion potential, the decrease in the corrosion current, and the change of the charge transfer resistance all demonstrate that the tropical marine atmospheric corrosion of the 7B04-T74 aluminium alloy presents a deceleration process, and the corrosion resistance is also proved from the side.

**Author Contributions:** Conceptualization, W.Z. and X.Y.; methodology, N.L. and Y.C.; validation, W.Z. and X.Y.; formal analysis, N.L. and L.H.; investigation, N.L. and L.H.; resources, W.Z.; data curation, N.L., M.Z. and Y.C.; writing—original draft preparation, N.L.; writing—review and editing, N.L., Y.C. and W.Z.; visualization, N.L. and M.Z.; supervision, X.Y.; project administration, N.L.; funding acquisition, W.Z. All authors have read and agreed to the published version of the manuscript.

**Funding:** This research is supported by the Basic Technical Research Project of China under Grant JSZL2018601B004.

**Institutional Review Board Statement:** Not applicable.

**Informed Consent Statement:** Not applicable.

**Data Availability Statement:** Not applicable.

**Conflicts of Interest:** The authors declare no conflict of interest.

## References

1. Claudet, J.; Bopp, L.; Cheung, W.W.; Devillers, R.; Escobar-Briones, E.; Haugan, P.; Heymans, J.J.; Masson-Delmotte, V.; Matz-Lück, N.; Miloslavich, P.; et al. A Roadmap for Using the UN Decade of Ocean Science for Sustainable Development in Support of Science, Policy, and Action. *One Earth* **2020**, *2*, 34–42. [[CrossRef](#)]
2. Zhou, B.; Liu, B.; Zhang, S. The Advancement of 7XXX Series Aluminium Alloys for Aircraft Structures: A Review. *Metals* **2021**, *11*, 718. [[CrossRef](#)]
3. Fuente, D. Corrosion of Aluminium, Aluminium Alloys, and Composites. *Encycl. Mater. Met. Alloys* **2022**, *1*, 160–169.
4. Koli, D.K.; Agnihotri, G.; Purohit, R. Advanced Aluminium Matrix Composites: The Critical Need of Automotive and Aerospace Engineering Fields. *Mater. Today Proc.* **2015**, *2*, 3032–3041. [[CrossRef](#)]
5. Dursun, T.; Soutis, C. Recent developments in advanced aircraft aluminium alloys. *Mater. Des.* **2014**, *56*, 862–871. [[CrossRef](#)]
6. Chen, S.Y.; Chen, K.H.; Peng, G.S.; Jia, L.; Dong, P.X. Effect of heat treatment on strength, exfoliation corrosion and electrochemical behavior of 7085 aluminium alloy. *Mater. Des.* **2012**, *35*, 93–98. [[CrossRef](#)]
7. Hou, S.; Zhu, Y.L.; Cai, Z.H.; Wang, Y.L.; Ni, Y.H.; Du, X.K. Effect of hole cold expansion on fatigue performance of corroded 7B04-T6 aluminium alloy. *Int. J. Fatigue* **2019**, *126*, 210–220.
8. Zhao, Q.Y.; Guo, C.; Niu, K.K.; Zhao, J.B.; Huang, Y.H.; Li, X.G. Long-term corrosion behavior of the 7A85 aluminium alloy in an industrial-marine atmospheric environment. *J. Mater. Res. Technol.* **2021**, *12*, 1350–1359. [[CrossRef](#)]
9. Sun, S.Q.; Zheng, Q.F.; Li, D.F.; Wen, J.G. Long-term atmospheric corrosion behaviour of aluminium alloys 2024 and 7075 in urban, coastal and industrial environments. *Corros. Sci.* **2009**, *51*, 719–727. [[CrossRef](#)]
10. Zhang, S.; Zhang, T.; He, Y.T.; Liu, D.X.; Wang, J.P.; Du, X.; Ma, B.L. Long-term atmospheric corrosion of aluminium alloy 2024-T4 in coastal environment: Surface and sectional corrosion behavior. *J. Alloys Compd.* **2019**, *789*, 460–471. [[CrossRef](#)]
11. Cai, Y.K.; Xu, Y.M.; Zhao, Y.; Ma, X.B. Atmospheric corrosion prediction: A review. *Corros. Rev.* **2020**, *38*, 299–321. [[CrossRef](#)]
12. Ji, Z.G.; Ma, X.B.; Zhou, K.; Cai, Y.K. An Improved Atmospheric Corrosion Prediction Model Considering Various Environmental Factors. *Corrosion* **2021**, *77*, 1178–1191. [[CrossRef](#)] [[PubMed](#)]
13. Cai, J.; Ming, L.; Luo, Z.; Tang, Z.; Bin, L.L.; Zhang, X.; Feng, L.U.; Tao, C. Study on accelerated tests for aluminium alloy atmospheric corrosion. *J. Chin. Soc. Corros. Prot.* **2005**, *25*, 262–266.
14. Zhang, Y.G.; Chen, Y.L.; Zhang, Y.; Bian, G.X.; Wang, C.G.; Wang, A.D. Initial corrosion behavior and mechanism of 7B04 aluminium alloy under acid immersion and salt spray environments. *Chin. J. Aeronaut.* **2022**, *35*, 277–289. [[CrossRef](#)]
15. Dan, Z.H.; Takigawa, S.; Muto, I.; Hara, N. Applicability of constant dew point corrosion tests for evaluating atmospheric corrosion of aluminium alloys. *Corros. Sci.* **2011**, *53*, 2006–2014. [[CrossRef](#)]
16. Vera, R.; Delgado, D.; Rosales, B.M. Effect of atmospheric pollutants on the corrosion of high power electrical conductors: Part 1. Aluminium and AA6201 alloy. *Corros. Sci.* **2006**, *48*, 2882–2900. [[CrossRef](#)]

17. Cao, M.; Liu, L.; Yu, Z.F.; Fan, L.; Li, Y.; Wang, F.H. Electrochemical corrosion behavior of 2A02 Al alloy under an accelerated simulation marine atmospheric environment. *J. Mater. Sci. Technol.* **2019**, *35*, 651–659. [[CrossRef](#)]
18. Peng, C.; Cao, G.W.; Gu, T.Z.; Wang, C.; Wang, Z.Y.; Sun, C. The corrosion behavior of the 6061 Al alloy in simulated Nansha marine atmosphere. *J. Mater. Sci. Technol.* **2022**, *19*, 709–721. [[CrossRef](#)]
19. Li, N.; Zhang, W.F.; Xu, H.; Cai, Y.K.; Yan, X.J. Corrosion Behavior and Mechanical Properties of 30CrMnSiA High-Strength Steel under an Indoor Accelerated Harsh Marine Atmospheric Environment. *Materials* **2022**, *15*, 629. [[CrossRef](#)]
20. Hao, L.; Zhang, S.X.; Dong, J.H.; Ke, W. Atmospheric corrosion resistance of MnCuP weathering steel in simulated environments. *Corros. Sci.* **2011**, *53*, 4187–4192. [[CrossRef](#)]
21. Zhang, Y.G.; Chen, Y.L.; Bian, G.X.; Zhang, Y. Electrochemical behavior and corrosion mechanism of anodized 7B04 aluminium alloy in acid NaCl environments. *J. Alloys Compd.* **2021**, *886*, 161231. [[CrossRef](#)]
22. Liang, M.X.; Melchers, R.; Chaves, I. Corrosion and pitting of 6060 series aluminium after 2 years exposure in seawater splash, tidal and immersion zones. *Corros. Sci.* **2018**, *140*, 286–296. [[CrossRef](#)]
23. Birbilis, N.; Zhu, Y.M.; Kairy, S.K.; Glenn, M.A.; Nie, J.F.; Morton, A.J.; Gonzalez-Garcia, Y.; Terryn, H.; Mol, J.M.C.; Hughes, A.E. A closer look at constituent induced localised corrosion in Al-Cu-Mg alloys. *Corros. Sci.* **2016**, *113*, 160–171. [[CrossRef](#)]
24. Ma, Y.; Zhou, X.; Huang, W.; Thompson, G.E.; Zhang, X.; Luo, C.; Sun, Z. Localized corrosion in AA2099-T83 aluminium–lithium alloy: The role of intermetallic particles. *Mater. Chem. Phys.* **2015**, *161*, 201–210. [[CrossRef](#)]
25. Yang, B.W.; Wang, Y.; Gao, M.Q.; Guan, R.G. The response of mechanical property to the microstructure variation of an Al-Mg alloy by adding tin element. *Mater. Sci. Eng. A* **2021**, *825*, 141901. [[CrossRef](#)]
26. Niverty, S.; Kale, C.; Solanki, K.N.; Chawla, N. Multiscale investigation of corrosion damage initiation and propagation in AA7075-T651 alloy using correlative microscopy. *Corros. Sci.* **2021**, *185*, 109429. [[CrossRef](#)]
27. He, L.Z.; Jia, P.F.; Zhang, L.; Cui, J.Z. Evolution of secondary phases and properties of 7B04 aluminium alloy during DC homogenization. *Trans. Nonferrous Met. Soc. China* **2016**, *26*, 319–327. [[CrossRef](#)]
28. Chen, Z.W.; Yan, K.; Ren, C.C.; Naseem, S. Precipitation sequence and hardening effect in 7A85 aluminium alloy. *J. Alloys Compd.* **2021**, *875*, 159950. [[CrossRef](#)]
29. Li, Z.H.; Xiong, B.Q.; Zhang, Y.A.; Zhu, B.H.; Wang, F.; Liu, H.W. Effects of the two-step ageing treatment on the microstructure and properties of 7B04 alloy pre-stretched thick plates. *Rare Metals* **2007**, *26*, 193–199. [[CrossRef](#)]

**Disclaimer/Publisher’s Note:** The statements, opinions and data contained in all publications are solely those of the individual author(s) and contributor(s) and not of MDPI and/or the editor(s). MDPI and/or the editor(s) disclaim responsibility for any injury to people or property resulting from any ideas, methods, instructions or products referred to in the content.